Tellus (2001), 53A, 300–316
Printed in UK. All rights reserved

TELLUS
ISSN 0280–6495

A troposphere–stratosphere–mesosphere general circulation model with parameterization of gravity waves: climatology and sensitivity studies

By EVGENY M. VOLODIN[1]* and GERHARD SCHMITZ[2], [1]*Institute of Numerical Mathematics of the Russian Academy of Science, Gubkina 8, Moscow 117951 GSP-1, Russia;* [2]*Institute for Atmospheric Physics, Schlossstrasse 6, Kuehlungsborn 18225, Germany*

(Manuscript received 5 July 1999; in final form 27 November 2000)

ABSTRACT

The climatology of the troposphere–stratosphere–mesosphere model of the Institute for Numerical Mathematics (INM) with the uppermost level at 0.003 hPa is presented. This model is vertically extended from the upper level of 10 hPa for the earlier version, and a drag parameterization due to internal gravity waves (GW) is included. The model describes the main features of the mesospheric circulation: decreasing and reversion of westerly and easterly winds, equatorward shift of the westerly wind maximum with height and reversal of the meridional temperature gradient in the upper mesosphere. The model underestimates to some extent the amplitude of wave number 1 for stationary waves in the winter hemisphere. The same holds for the internal low-frequency variability in the winter stratosphere. The sensitivity of the model climate is studied with respect to the inclusion of orographic gravity wave drag and the variation of the source height of internal gravity waves.

1. Introduction

Numerical modeling of the atmospheric processes in the troposphere is well developed, and there are many comprehensive atmospheric general circulation models (AGCMs) capable of describing the main observed features of the atmospheric climate up to 10–20 km height. Only a few models with the upper boundary above the stratopause have been developed (Hamilton, 1996), and the main features of the climate state in the stratosphere and mesosphere are remarkably different among these models. One of the reasons for this discrepancy is an insufficient knowledge of momentum transfer induced by gravity wave breaking. The basic points of the theory of gravity waves (GW) and their saturation in the middle atmosphere have been proposed by Lindzen (1981). Orography, convection and vertical wind shear are the main sources of GW, but their geographical distribution and magnitude is not yet known with appropriate accuracy. An overview of gravity wave parameterizations in global climate models is given in Hamilton (1997).

In some of the troposphere–stratosphere–mesosphere (TSM) models, Rayleigh friction is used: the early version of the ECHAM model (Manzini and Bengtsson, 1996), the Berlin TSM model (Langematz and Pawson, 1997; Pawson et al., 1998), the UKMO's Unified Model (Butchart and Austin, 1998; Swinbank et al., 1998). The standard version of the GFDL SKYHI model (Hamilton et al., 1995) has no parametrisation of subgrid-scale gravity wave effects.

The MACCM2 model (Boville, 1995) includes

* Corresponding author.
e-mail: volodin@inm.ras.ru

Rayleigh friction and the orographic component of GW drag (OGWD). Some model groups use a saturation criterion for the parameterization of non-orographic GW: the GISS model (Rind et al., 1988a), the ARPEGE model (Christiansen et al., 1997) and extended UGAMP GCM, Norton and Thuburn (1997).

Hines (1997a, b) developed a parameterization of the non-orographic GW drag, the so called Doppler-spread parameterization of gravity wave drag (DSP GWD) which is used in climate models by Manzini et al. (1997a, b) and McFarlane et al. (1997). These models reproduce the observed zonal mean wind and temperature in the stratosphere and mesosphere quite well, but the results are very sensitive to the choice of some input parameters for the DSP GWD (Manzini and McFarlane, 1998). Often, such parameters cannot be chosen in a simple way because the choice depends on the model formulation. Therefore, it seems that the development of new TSM models and the consideration of the sensitivity of model results to the parameterization of small-scale wave processes in the stratosphere and mesosphere is a subject of continuous interest.

The aim of this paper is to show the ability of INM AGCM to describe the observed climate of the stratosphere and mesosphere with perpetual January and July simulations. The sensitivity of the model climate to gravity wave parameterization is studied.

The outline of the paper is follows. The model is described in Section 2. Model experiments and observational datasets are discussed in Section 3. Section 4 presents the climatology of the model and a comparison with observations. Sensitivity experiments are described in Section 5, a discussion and conclusions can be found in Section 6.

2. Model description

The model used in this study is an extension of the INM AGCM described in Alekseev et al. (1998) to upper stratospheric and mesospheric heights. The original model contains 21 levels in σ-coordinates from the surface up to 10 hPa. The troposphere–stratosphere–mesosphere model has 39 levels in σ-coordinates from the surface up to 0.003 hPa. In the upper stratosphere and mesosphere, the distance between the layers is approximately 3 km.

Finite difference dynamics employs the C-grid of Arakawa and Lamb (1981). Prognostic variables are zonal and meridional wind, temperature, specific humidity and surface pressure. The horizontal resolution is 5° in longitudinal and 4° in latitudinal direction. In polar regions, Fourier filter applies in the longitudinal direction to remove short waves and to avoid numerical instability. Semi-implicit time stepping is used with a time step of 7.5 min.

The model includes a 4th-order horizontal diffusion applied to the horizontal momentum, temperature and specific humidity. The diffusion coefficient C for the horizontal momentum depends on the wind speed $|V|$ and is calculated as follows: $C = C_0 \cdot \max(V_{\min}, |V|)$ with $C_0 = 4.29 \times 10^{15}\ \mathrm{m}^3$ and $V_{\min} = 16\ \mathrm{ms}^{-1}$. No explicit dependence of the diffusion coefficient on height is imposed. For temperature and specific humidity, the diffusion coefficient is $C/2$.

The radiation parameterization follows Galin (1998). Calculation of radiation fluxes is performed in 10 spectral intervals for the long-wave part of the spectrum and in 18 spectral intervals for the short-wave part. Absorption due to H_2O, CO_2, O_3, O_2, CH_4, N_2O, aerosol and clouds is taken into account. Cloud amount, cloud water and ice are calculated diagnostically. The ozone concentration is prescribed and depends on latitude and pressure according to Wang et al. (1995). Absorption of short-wave radiation by ozone is considered in 8 spectral intervals (Briegleb, 1992). The infrared line 9.6×10^{-6} m of ozone absorption is considered separately (Chou and Kouvaris, 1991). Prescribed uniform distributions of CO_2, O_2, CH_4 and N_2O are utilized. A 3-h time step for the calculation of radiation processes is used. The diurnal solar cycle is included.

Parameterization of gravity wave drag consists of 2 independent parts: OGWD by Palmer et al. (1986) and DSP GWD by Hines (1997a, b). Here, we present a short description of DSP GWD applied in the model. The notations are the same as in Hines (1997a, b).

The gravity waves are assumed to be generated at a single prescribed level i. The vertical wave m_k at level k results from that at the initial level m_i according to

$$N_k m_k^{-1} = N_i m_i^{-1} + V_i - V_k - v_k. \tag{1}$$

N is the buoyancy frequency, V and v are the large-scale and the wave perturbation wind projections onto the azimuth under consideration. Waves with vertical wave numbers $m_k > m_{\max}$ are assumed to become unstable and this results in a momentum deposition. The maximum wave is given by:

$$m_{\max} = N_i(\Phi_1 \sigma_{jk} + \Phi_2 \sigma_{hk} + V_k - V_i)^{-1}, \qquad (2)$$

where σ_{jk} denotes the wind rms (root mean square) due to gravity waves in the azimuth j, σ_{hk} the wind rms in all the directions, and Φ_1, Φ_2 are fudge factors of the order of 1. The wind rms is calculated using the wave spectrum at the current level.

The turbulence resulting from wave breaking is parameterized through a vertical diffusion (VD) which is applied to the horizontal wind and temperature. For temperature, the VD coefficient is restricted by a maximum value of 250 m^2/s. The vertical heat flux resulting from gravity waves is taken into account according to Hines (1997a, b).

The initial vertical wave spectrum is assumed to be linear ($s = 1$). The minimum initial vertical wave is $m_m = 10^{-4}\, m^{-1}$. The source of gravity waves is located at 500 hPa in the standard model version, assuming that troposphere cloudness is the main source of gravity waves. Initial gravity wave rms wind speed $\sigma_{hi} = 1.75\, ms^{-1}$ with isotropic distribution. This value is the same as in Manzini et. al. (1997a, b). The effective horizontal wave is $k^* = 2.5 \times 10^{-5}\, m^{-1}$. The number of azimuths considered is 12. The fudge factors are specified as follows: $\Phi_1 = 1.5$ (directional rms coefficient), $\Phi_2 = 0.3$ (total rms coefficient), $\Phi_5 = 1.0$ (coefficient for internal energy), $\Phi_6 = 0.25$ (coefficient for VD).

Parameters and fudge factors are chosen within the range recommended in Hines (1997a, b). They are not far from that used in McFarlane et al. (1997), and in Manzini et al. (1997a, b) except for Φ_5, Φ_6 that are neglected in those studies.

The present AGCM employs no additional Rayleigh friction or relaxation. The parameterization of deep and shallow convection is taken into account according to Betts (1986). Soil and vegetation processes are parameterized as in Volodin and Lykossov (1998). Sea-surface temperature and the amount of sea ice are prescribed. Land surface temperature, snow amount, soil temperature and humidity are calculated prognostically.

In summary, the only difference in the parameterizations of the model physics between the present TSM AGCM and the original troposphere–stratosphere AGCM (Alekseev et al., 1998) is the inclusion of the DSP GWD and the associated VD according to Hines (1997a, b).

3. Model experiments and observational datasets

All model runs have been performed under perpetual January or perpetual July conditions. The choice of perpetual month regime was defined by minimization of computer time for control and sensitivity experiments. Comparison of model data for January and July from 10-year run with the seasonal cycle (not presented) and the data for the perpetual month regime shows that the difference between these 2 runs is small for time mean state and month-to-month variability. So, data for perpetual months discussed here are capable of describing model climate.

The model sensitivity to GW parameterization is studied with 3 different model setups. In the standard model, (M1) DSP GWD is employed while OGWD is neglected. The gravity wave source is located at 500 hPa. The 2nd model setup M2 is identical to M1 except that OGWD is taken into account additionally. M3 differs from M2 by locating the gravity wave source at 150 hPa.

The M1 and M2 model runs consist of 30-month time series for perpetual January conditions and the 10-month time series for perpetual July conditions. The M3 has been integrated for 10 months and only for perpetual January conditions. All 30 (10) months of integration are taken into account when mean state and variability are calculated.

Comparison of the model climatology with the observations utilizes 3 different datasets. The observations of CIRA-86 (Fleming et al., 1990) are used for the zonal mean temperature and zonal mean zonal wind fields in the upper stratosphere and mesosphere. The climatology of Randel (1992) provides a reference for the amplitudes of planetary waves, the stationary wave momentum and heat fluxes and the month-to-month variability. Both datasets contain geostrophic winds only, so, for a better comparison of the model climate with the observations in the troposphere and low stratosphere, NCEP/NCAR reanalysis data (Kalnay et al., 1996) at 1000–10 hPa for 1979–1997 years are taken into consideration.

For the calculation of empirical orthogonal functions (EOFs), monthly mean data from January integrations of experiments M1 and M2 are used. These are compared with EOFs calculated from the Randel monthly mean data for December, January, February and March with the mean annual cycle removed. For such a calculation, all the data are weighted by $(\cos\phi\Delta P)^{0.5}$, where ϕ is latitude and ΔP is the thickness of the pressure level. After the calculation, the EOFs are divided by this weight.

4. Model climatology

4.1. *Zonal mean wind and temperature*

January zonally averaged temperature and zonal wind of the control run and observations of CIRA-86 (Flemming et al., 1990) are presented in Fig. 1. The main features of the stratospheric and mesospheric circulation are well reproduced. In the upper mesosphere, the model shows a strong decrease with height for the westerly winds in the winter hemisphere and the easterly winds in the summer hemisphere. An equatorward shift of westerly winds with height in the winter stratosphere and mesosphere is also obvious. The location of the westerly wind maximum in the winter hemisphere is somewhat below the observed one, and its intensity is somewhat stronger than in the observations. The reversal of the temperature gradient in the upper mesosphere is reproduced by the model, even though the overall temperature difference between the summer and winter pole is underestimated. The simulated stratopause is 5–10 K warmer than observed. This discrepancy is most pronounced in the northern high latitudes. In the upper mesosphere, the global mean temperature produced by the model is 5–10 K below the observations.

Fig. 2 shows the observed and simulated zonal winds and temperatures for July. The winter hemispheric wind maximum simulated by the model is too weak and located at lower altitudes in comparison with the observations. The tilt of the winter hemispheric jet is weaker in the model than in the observations. In the summer hemisphere, the model easterly wind in the mesosphere is somewhat too strong around the tilted axis of the jet, but its meridional extension is much smaller. One of major failings is that in the summer hemisphere, westerlies extend too high into the stratosphere. The model temperature in the mesosphere summer hemisphere represents the observations qualitatively.

In the following, we consider the zonal mean of the zonal wind and temperature in the troposphere and low stratosphere. Fig. 3 shows the differences between the control run (M1) and the NCEP/NCAR reanalysis for January and July. The main differences in the temperature field are located in the tropopause height region. In the tropics, the temperature is 2–6 K larger than that observed with the maximum deviation near 100 hPa. This discrepancy between the INM AGCM and the observations was reduced from 8–12 K to 2–6 K by a reduction of the optical thickness of the upper tropical clouds. Near the midlatitude and polar tropopause, the model temperature is 5–10 K smaller than that observed.

There is also a discrepancy between the observed and the model temperature in the polar southern stratosphere. For July conditions, an overestimation of the temperature by 15 K appears. This shortcoming is connected with an underestimation of the winter hemispheric winds in the upper stratosphere. Probably the reason lies in excessive DSP GWD just above the maximum of westerly winds. This drag seems to produce a strong meridional circulation accompanied by enhanced descent and adiabatic warming in the extratropics.

For January, the polar southern hemisphere is too cold up to 10 K. The overestimation of the temperature in the northern midlatitudes in the lower troposphere in July and the associated discrepancy in the wind structure can be explained by dry and hot soil due to perpetual July conditions. In agreement with a cold polar tropopause and a warm tropical tropopause, there is a westerly wind bias in the stratosphere in the midlatitudes. This shortcoming is present in both hemispheres and in both seasons. In the lower tropical stratosphere the intensity of easterly wind is overestimated by 10–15 ms^{-1} in January and July. The overall differences between the TSM model climate and the NCEP/NCAR reanalysis are not far from those described in Alekseev et al. (1998).

4.2. *Stationary waves and wave fluxes*

The amplitudes of wave numbers (k) 1 and 2 of the geopotential in January are presented in Fig. 4.

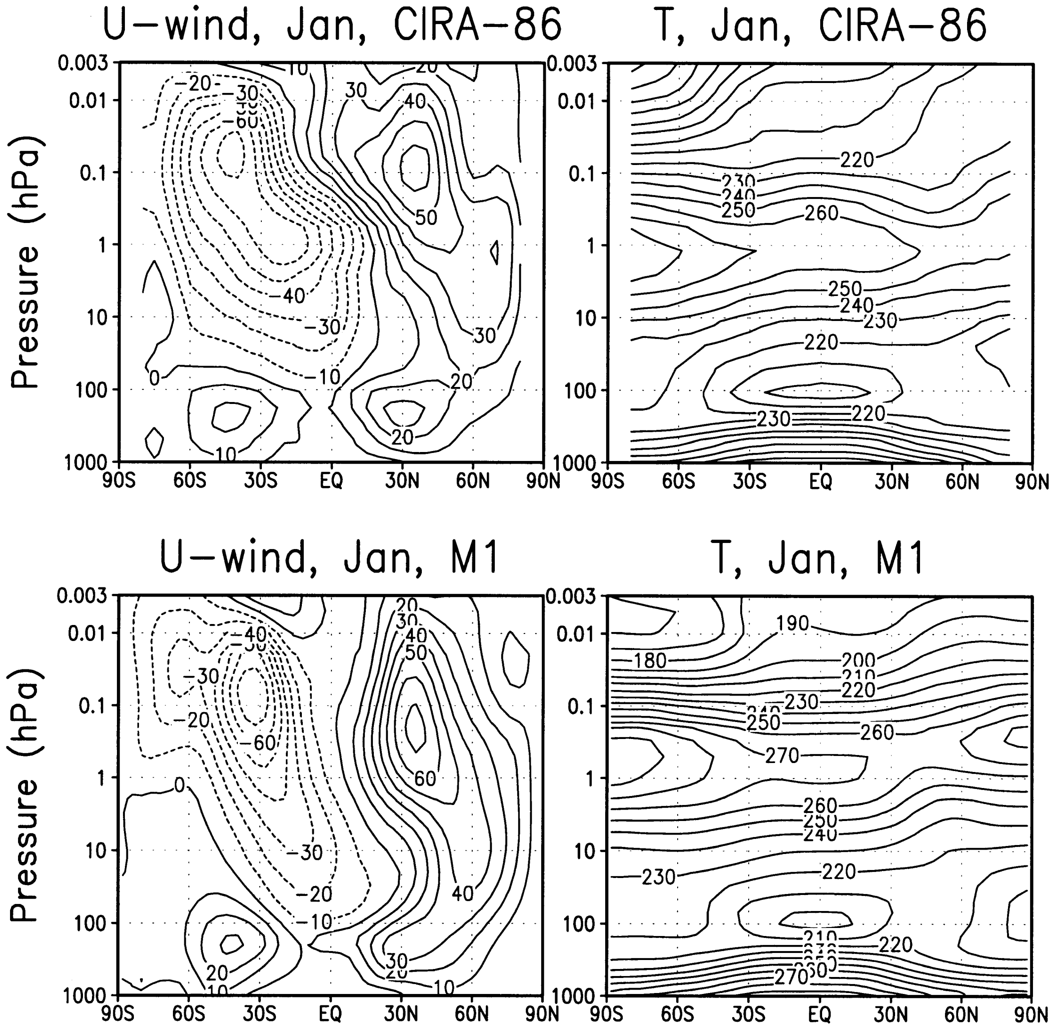

Fig. 1. Zonal mean zonal wind (left) and temperature (right) in January of CIRA-86 (top) and M1 (bottom). Contour interval is 10 ms^{-1} for the wind and 10 K for temperature. Negative contours are dashed.

The model underestimates the amplitude of wave $k=1$ and overestimates to some extent the amplitude of wave $k=2$. Probably this difference results from the same shortcoming in the upper troposphere, where the amplitude of wave $k=1$ is weaker, and the amplitude of wave $k=2$ is stronger than that for the observations.

In July (Fig. 5) in the winter hemisphere, the amplitude of wave $k=1$ is 1.5–2.0 times weaker in the model than that for the observations. The amplitude of wave $k=2$ is not far from the observed one. In the summer hemisphere, the amplitudes of both waves are in agreement with the observations.

The observed stationary meridional fluxes of westward momentum and heat are presented in Fig. 6. The momentum flux in M1 in the stratosphere is in a good agreement with the observations, Randel (1992). The momentum flux for $k=1$ is too weak, whereas momentum fluxes for $k=2$ and $k=3$ are much stronger in the model than that for the observations (not shown).

In the stratosphere, the simulated stationary heat flux is half of that observed, and the position

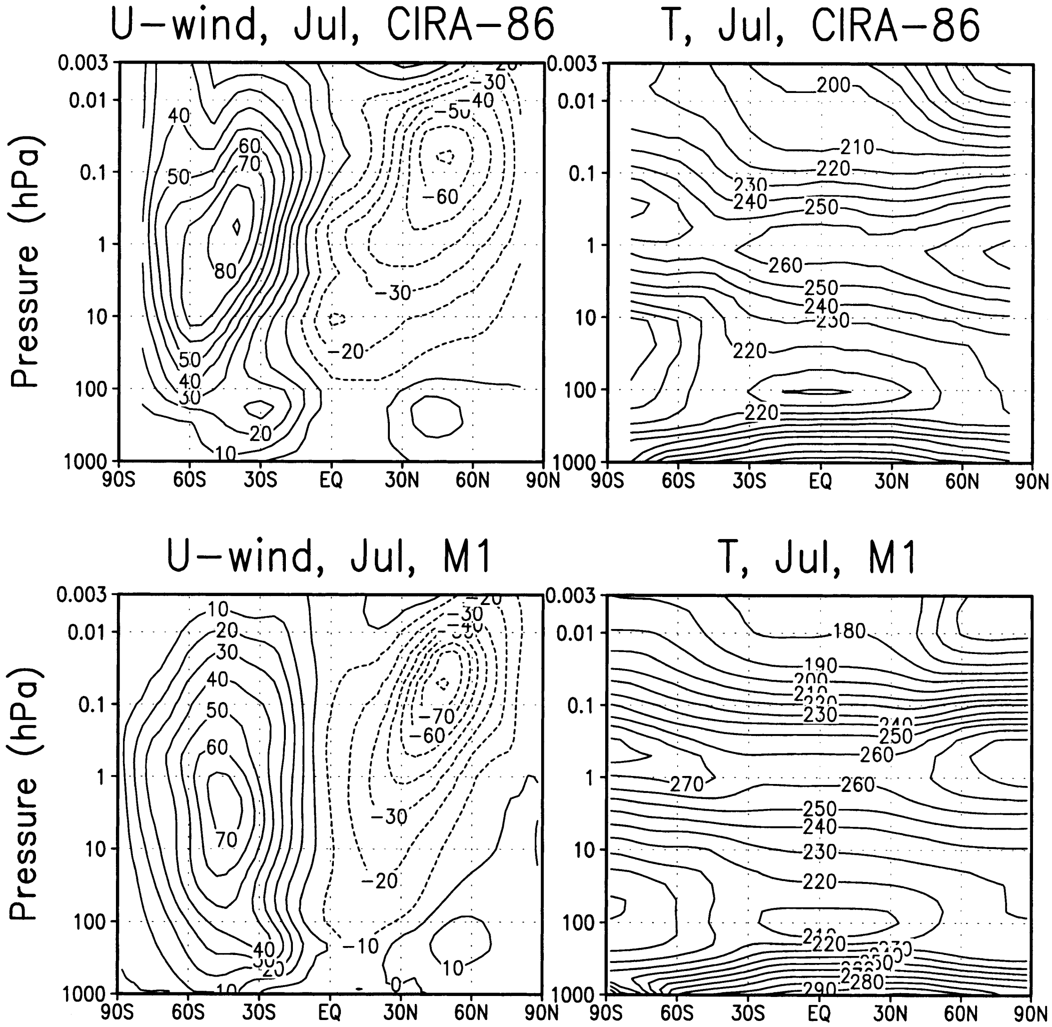

Fig. 2. Zonal mean zonal wind (left) and temperature (right) in July of CIRA-86 (top) and M1 (bottom). Contour interval is 10 ms^{-1} for the wind and 10 K for temperature. Negative contours are dashed.

of the maximum in the model is shifted 20° south in comparison with the observations.

4.3. Month-to-month variability of zonal mean wind and temperature

The rms variabilities of the zonal and monthly mean zonal wind and temperature are calculated for perpetual January conditions based on the 30-month simulations with M1. The data of Randel (1992) for the years 1979–1997 have been used for monthly mean zonal wind and temperature rms calculations and are shown together with the model results in Fig. 7.

The model rms of zonal mean wind has its maximum value in the northern hemispheric upper stratosphere and mesosphere around 45°N. The maximum for the observations is located near 55°N. The amplitude of the zonal wind variability in the model is smaller than that in the observations.

The root mean square of the temperature has its maximum value in the northern polar latitudes of the stratosphere and mesosphere. The amplitude

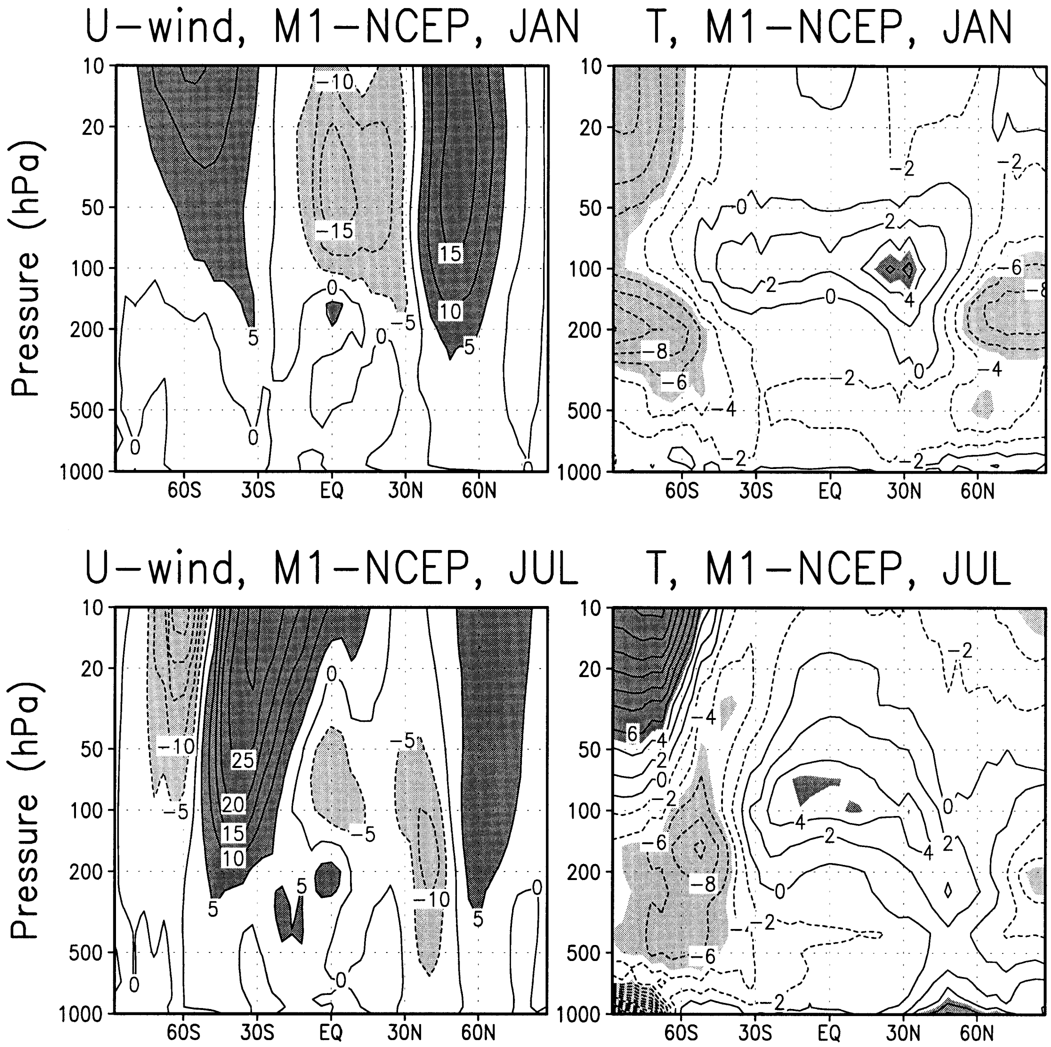

Fig. 3. The difference between data of M1 and NCEP/NCAR reanalysis for zonal mean zonal wind (top) and temperature (bottom) in January (left) and July (right). Contour interval is 5 ms^{-1} for the wind and 2 K for the temperature. The differences above 5 ms^{-1} and above 5 K are paint over. Negative contours are dashed.

is larger in the observations than in the model results.

The underestimation of the model month-to-month variability can be related to the absence of low-frequency variability resulting from external forcing. Furthermore, the model simulates the planetary wave $k = 1$ amplitudes too weakly, which may influence the model variability.

For a better understanding of the structure of low-frequency model variability, the first EOFs of zonal mean zonal wind and temperature are calculated.

The first EOFs of the zonal wind for the model results and the observations (Fig. 8) have their maximum values in the northern hemisphere. These EOFs indicate variability of the zonal wind with opposite signs in the northern hemispheric subtropics and high latitudes throughout the troposphere and stratosphere, with maximum at 10 hPa for the model results as well as for the

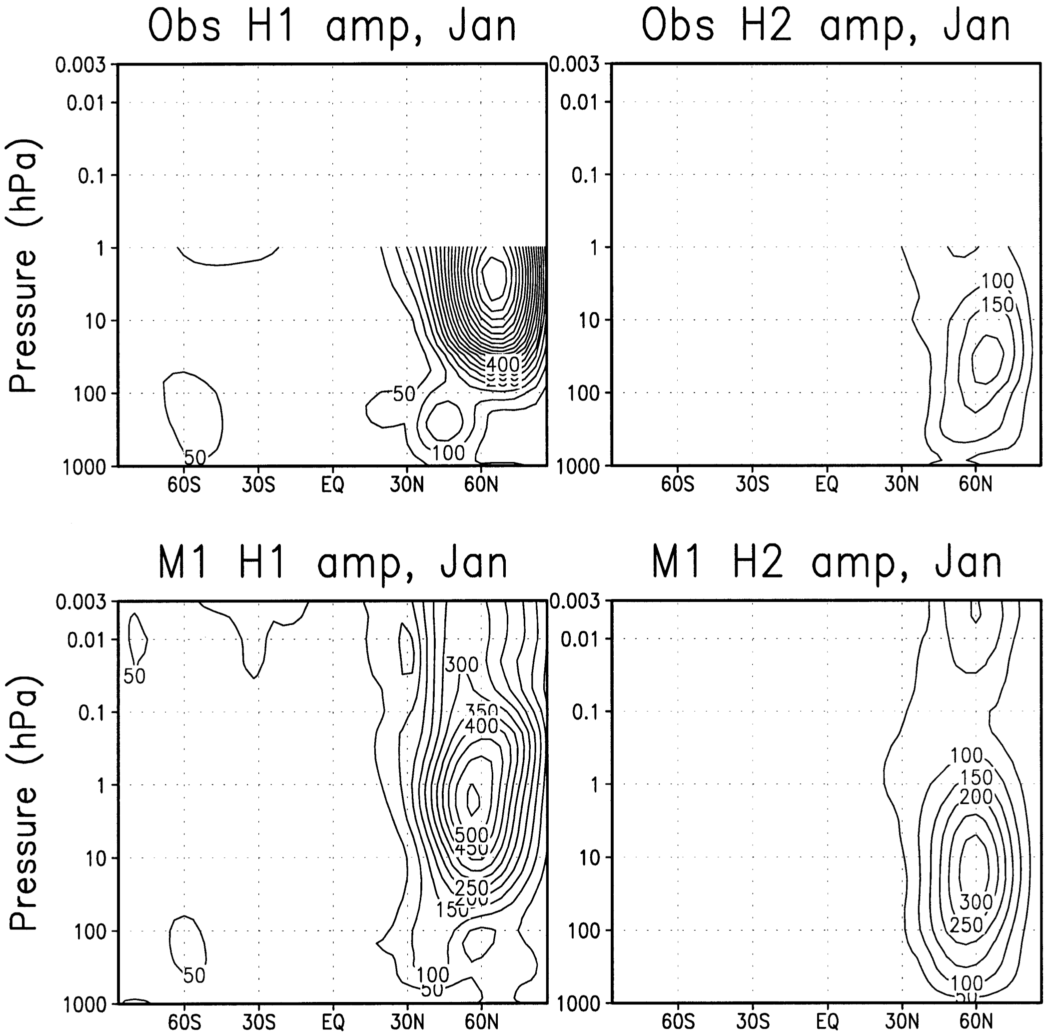

Fig. 4. The amplitude of stationary wave 1 (left) and 2 (right) of the geopotential in January, data of Randel (1992) (top) and M1 (bottom). Contour interval is 50 gpm.

observations. In the model results, this structure yields up to 1 hPa. In the mesosphere, the model EOF has a completely different structure.

The first EOFs of the temperature for the observations and the model (Fig. 8, right) represent anomalies of the temperature in high latitudes around 50 hPa and 1 hPa with different signs. Temperature anomalies in low latitudes are of the opposite sign and of smaller amplitude with respect to those at high latitudes.

The model represents well the structure of the EOF for the observed temperature.

5. Sensitivity experiments to gravity wave parameterization

Now we consider the sensitivity of the model climate to inclusion of OGWD and to variation of the initial level for DSP GWD. The differences between the OGWD model experiments M2 and M1 for the January zonal wind and temperature are shown in Fig. 9. The OGWD leads to a weaker zonal wind in the stratosphere and mesosphere at 40N–50N and stronger zonal wind in the stratosphere at 0N–30N and 60N–80N. In the temper-

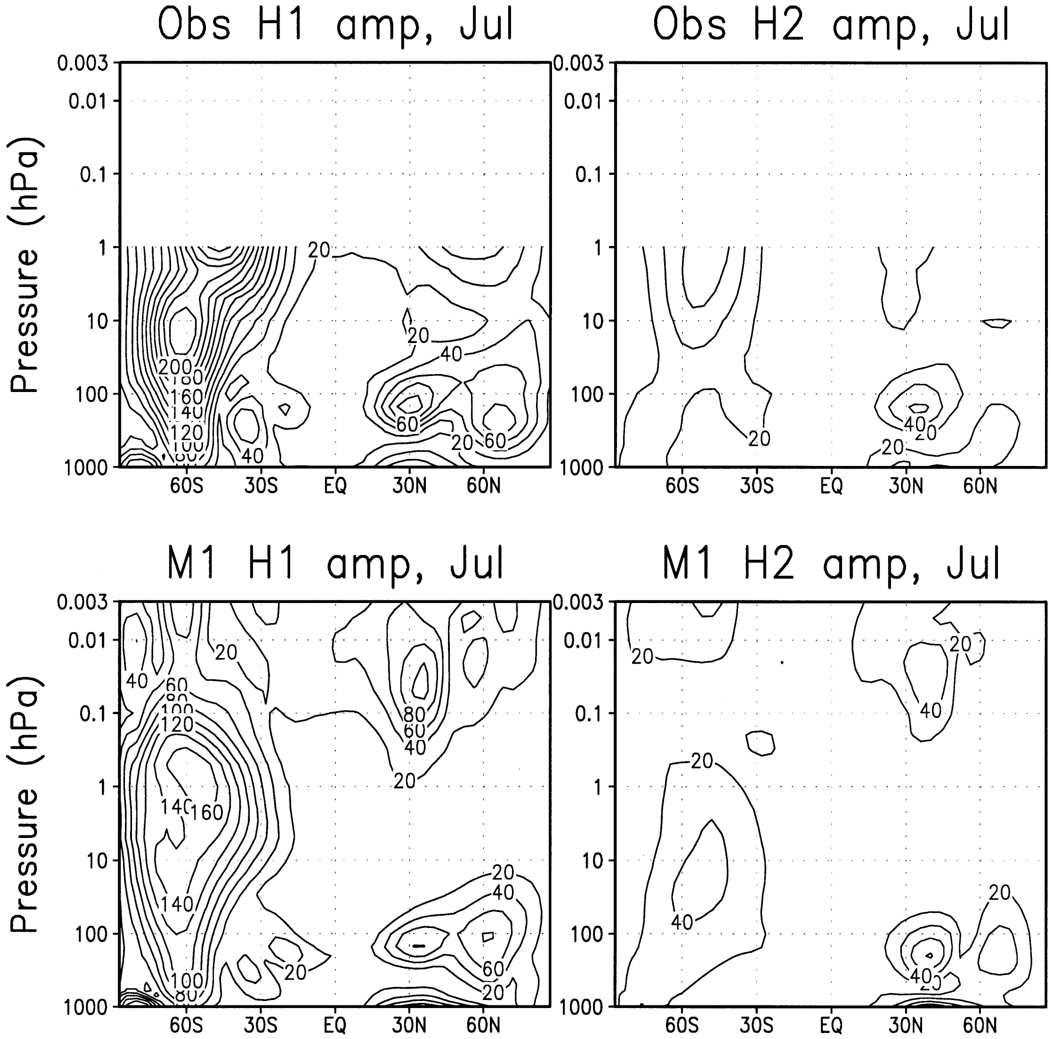

Fig. 5. The amplitude of stationary wave 1 (left) and 2 (right) of the geopotential in July, data of Randel (1992) (top) and M1 (bottom). Contour interval is 20 gpm.

ature field, the most pronounced feature is a warming of the midlatitude stratopause and a cooling of the tropical stratopause. Due to inclusion of OGWD, the temperature decreases in the upper stratosphere and lower mesosphere in tropics up to 2–4 K and increases in the northern midlatitudes up to 5–10 K. Such temperature changes are induced by enhancement of upward movement in the tropics and downward movement in the northern midlatitudes (not shown).

The amplitudes of wavenumbers $k=1$ and $k=2$, and the stationary meridional fluxes of momentum and heat in the stratosphere in January are weaker in M2 than in M1 (not shown), probably due to a direct damping of waves by OGWD. In the troposphere, the response of the model to inclusion of OGWD is weak.

Zonal mean zonal wind and temperature for M3 and the response of the model to the shift of the initial height for DSP GWD from 500 hPa to 150 hPa are shown in Fig. 10. One can recognize an increase of westerlies and decrease of easterlies

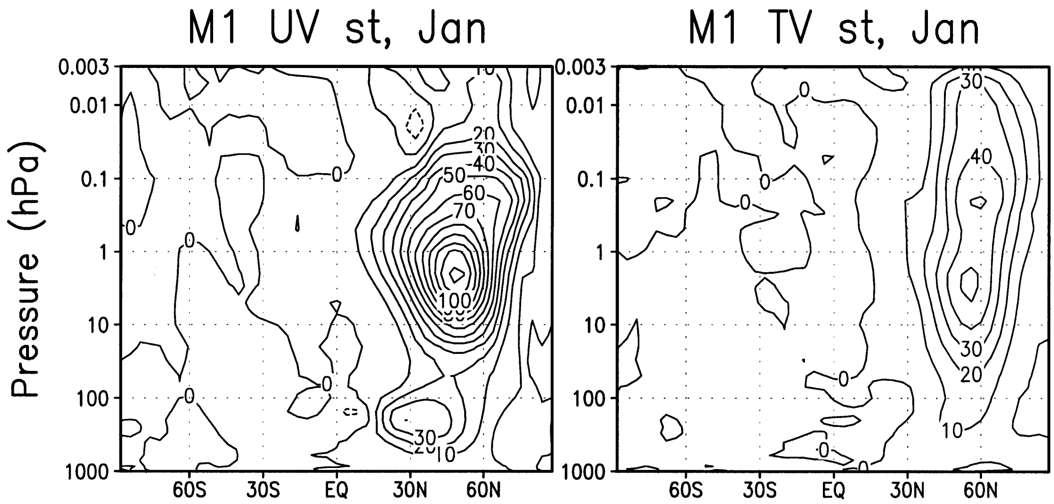

Fig. 6. Zonal momentum (left) and heat (right) meridional stationary flux in January, data of M1. Contour interval is 10 $m^2 s^{-2}$ for momentum flux and 10 K ms^{-1} for heat flux. Negative contours are dashed.

almost everywhere in the stratosphere and mesosphere (except for the southern polar mesosphere) with a maximum anomaly of 70 ms^{-1} near the maximum of easterly winds for M1 (Fig. 1). Also a warming up to 10–20 K is visible in the mesosphere and a cooling of 5–15 K in the polar upper stratosphere. The temperature gradient between the northern and southern upper mesosphere is somewhat reduced in M3 in comparison with M2.

Fig. 11 shows zonal mean tendencies for zonal momentum induced by DSP GWD, VD and OGWD in January for the M2 experiment. In the mesosphere, DSP GWD gives the most important contribution. The influence of vertical diffusion is 3–5× weaker. OGWD is the most important factor in the upper stratosphere and lower mesosphere of the winter hemisphere.

6. Discussion and summary

In this paper, the climatology of INM TSM AGCM for perpetual January and perpetual July regimes is presented. The comparison of TSM AGCM results with the observations shows that the model is capable of reproducing the main features of the stratospheric and mesospheric circulation. The zonal wind in the stratosphere and mesosphere is described, including decrease and reversal in the mesosphere and equatorward tilt of the wind maximum in the winter upper stratosphere. The reversal of the temperature gradient in the upper mesosphere is also represented.

A discrepancy between the model and the observational temperature near the tropopause is a common problem. In particular, a cold bias at the polar tropopause in the AGCM climate is also mentioned in Manzini et al. (1997a, b), Hamilton et al. (1995) and Boville (1995). One of the reasons for the discrepancy may be poor understanding of the cloud optical properties in the upper troposphere. Non-closure of the model tropospheric subtropical jet can also be addressed on this point. Such a cold bias near the polar tropopause and also a warm bias near the tropical tropopause lead to an overestimation of the westerly zonal mean wind component in the midlatitudes in the upper troposphere and stratosphere for both seasons and for both hemispheres. Warm model bias near the tropical tropopause is stronger in comparison with ECMWF reanalysis or radiosonde data (Pawson and Fiorino, 1998), than in comparison with NCEP reanalysis.

These differences between the model and the observations are almost the same for the TSM model and for the model with the upper boundary at 10 hPa (Alekseev et al., 1998). Additional model runs with a higher vertical resolution around the tropopause (not shown) do not indicate that

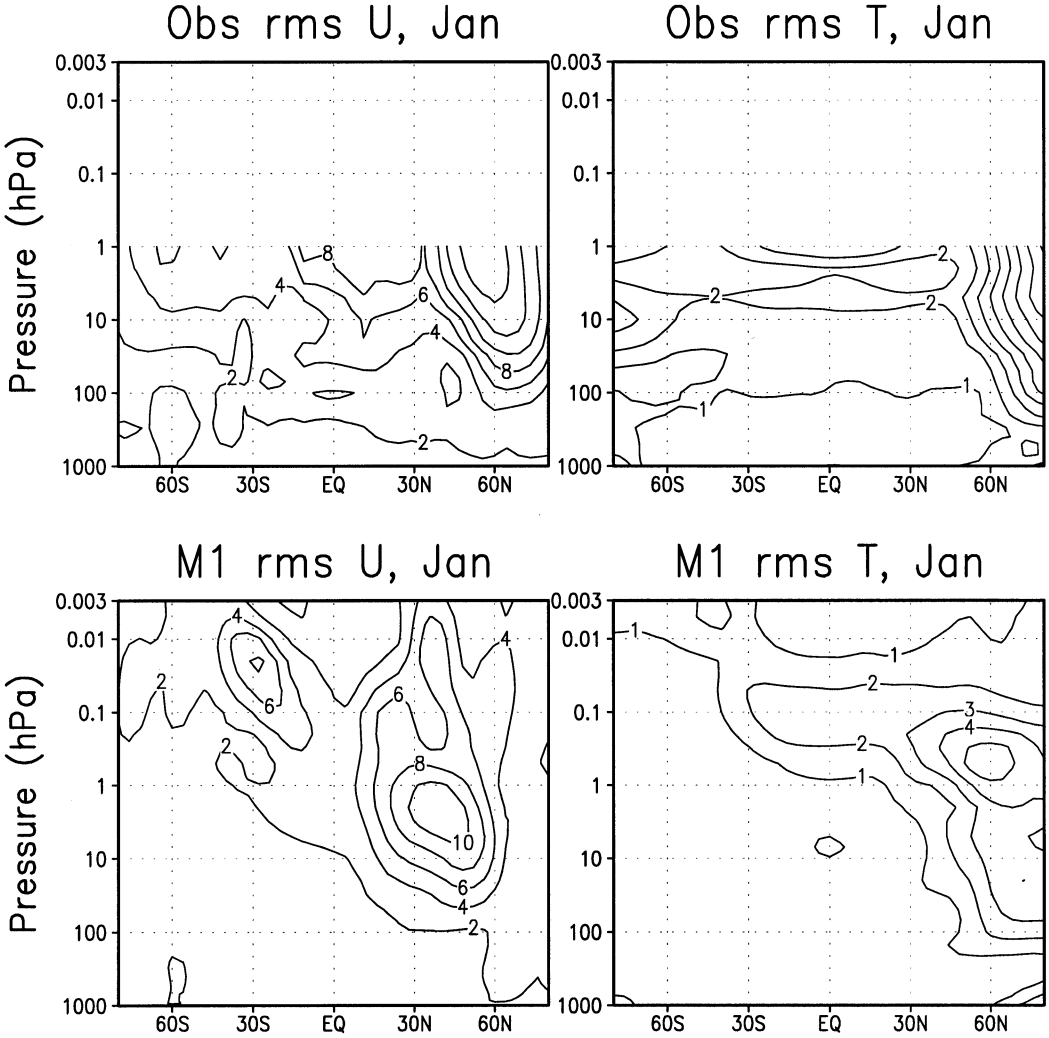

Fig. 7. Root mean square of monthly and zonal mean zonal wind (left) and temperature (right) in January, data of Randel (1992) (top) and M1 (bottom). Contour interval is 2 ms^{-1} for the wind and 1 K for temperature.

warm and cold biases around the tropopause are sensitive to the vertical resolution.

The comparison of the model zonal wind with the observations shows that in July, the maximum of the westerly stratosphere–mesosphere jet in the southern hemisphere is located at lower heights than that in the observations. This shortcoming depends on an excessive DSP GWD, which leads to large negative zonal wind tendencies just above the wind maximum. It seems that an analogous shortcoming occurs with the M2 model for January. If OGWD is included, the model shows a decrease of the zonal wind around 0.1 mb, 40°N, and an increase just below. Probably further improvement of the model can be achieved if we consider OGWD in the standard version and reduce DSP GWD for westerly winds.

The sensitivity experiment concerning the change of the initial level for DSP GWD shows that the initial level is one of the crucial points in simulating the mesospheric climate. This conclusion is in accordance with the theory of GW

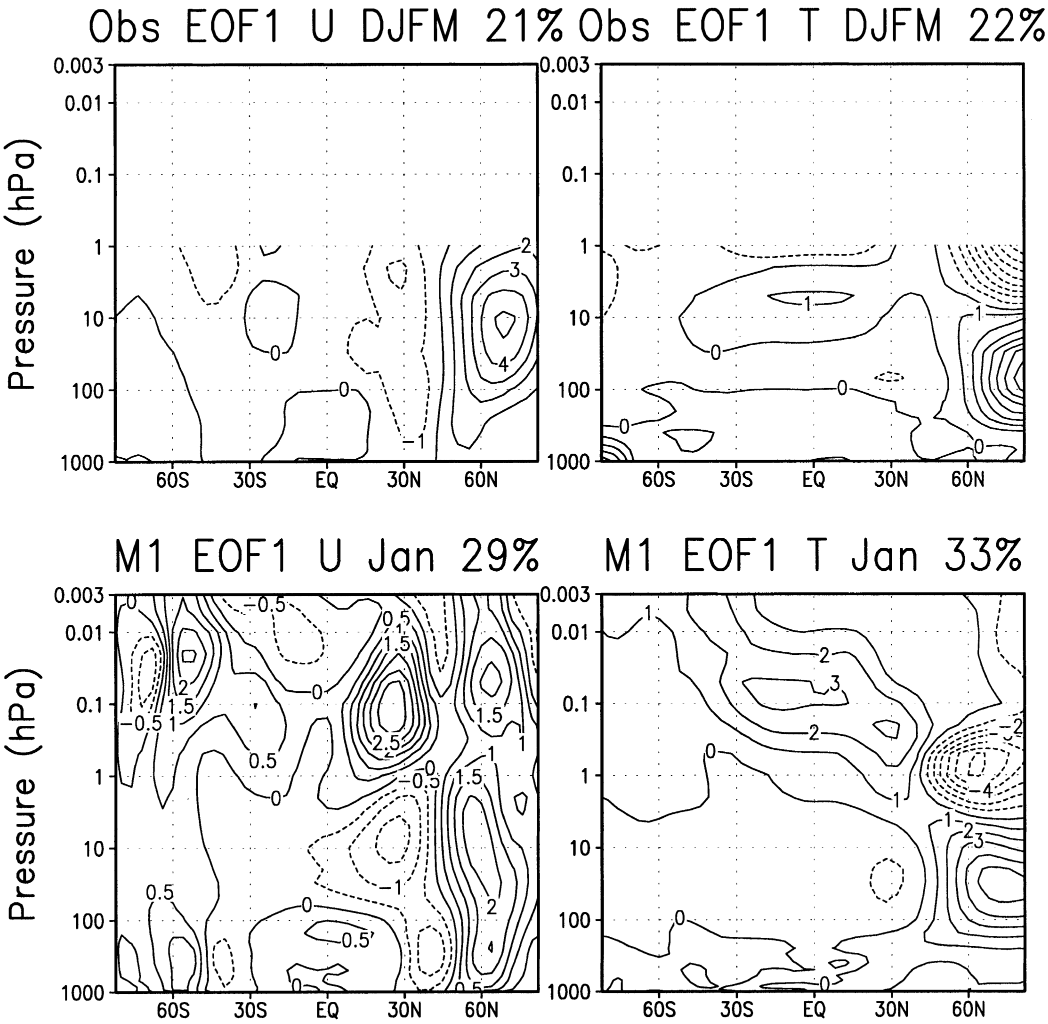

Fig. 8. The first EOF of monthly and zonal mean zonal wind (left) and temperature (right) in December, January, February and March, data of Randel (1992) (top) for M1 in January (bottom). Units are arbitrary. The variability explained by the EOFs in percents is written above each EOF figure. Negative contours are dashed.

proposed by Lindzen (1981). The model response in the zonal mean zonal wind (Fig. 10) is not far from the corresponding results of Manzini and McFarlane (1998). In that study, a change of the source height of GW from the surface to 110 hPa leads to an acceleration of the westerly wind everywhere in the mesosphere. The authors discussed that the reason for such behavior depends on the gravity wave absorption at the height of maximum westerly wind in the upper troposphere. The absorption of the waves with the eastward horizontal momentum component occurs if the initial level is placed below the westerly wind maximum, but it is not the case if the initial level is placed above the maximum.

The temperature in the polar winter stratosphere decreases by up to 15 K if the initial level is raised to 150 hPa. This is in agreement with the results of Manzini and McFarlane (1998).

The temperature in the mesosphere in model M3 is higher than that in M2. This is due to a weaker vertical diffusion in the mesosphere in M3,

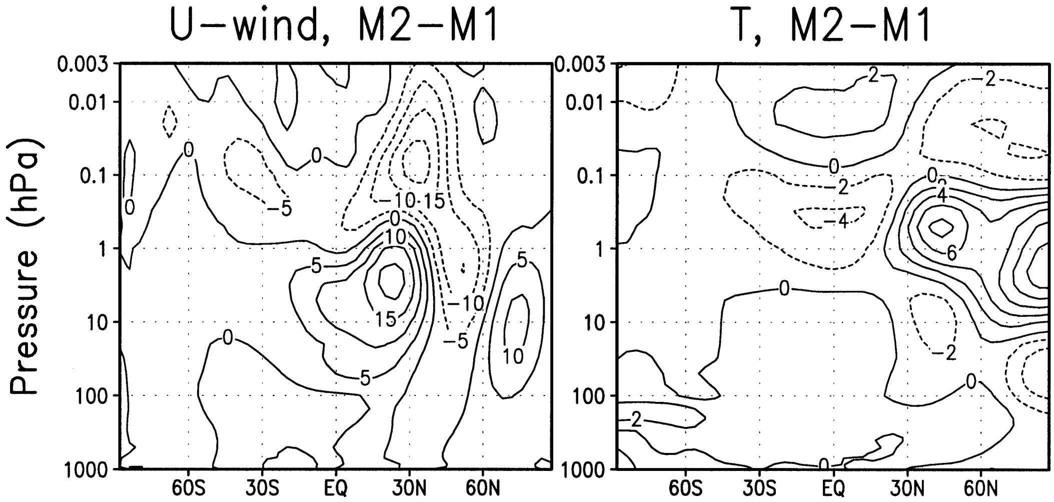

Fig. 9. The difference of zonal wind (left) and temperature (right) between M2 and M1. Contour interval is 5 ms^{-1} for the wind and 2 K for the temperature.

which leads to a reduced cooling. Let us explain this point in detail. For both models, M2 and M3 initial wind rms σ_i is the same, but is prescribed at different levels. In the absence of breaking, the wind rms σ induced by GW propagated upward increases with height as $\rho^{-0.5}$, where ρ means air density. Thus, we have different wind rms in M2 and M3 at the same level, greater for M2 and weaker for M3. The VD coefficient in the parameterization of Hines (1997a, b) is proportional to $\sigma^{7/3}$. Therefore, in M3, the VD coefficient at the same level should be less than that in M2. Potential temperature increases with height, so vertical diffusion induces cooling in the stratosphere and mesosphere, and this cooling is stronger in M2 than that in M3.

In our model, the cooling due to VD in the mesosphere is of the order of 10 K day^{-1}. It is not far from the results of Rind et al. (1988a, b), which have used another GWD parameterization, but the vertical diffusion with the coefficient calculated in GWD parameterization is applied to the horizontal wind and temperature.

The sensitivity experiments show that it is possible to vary the model climate in the mesosphere in a wide range by varying a few parameters in DSP GWD. Taking also into account large uncertainties of these parameters, one can conclude that additional studies concerning the source height for GW, initial wind rms for GW and VD coefficient in the mesosphere are necessary for further improvement of TSM GCMs. One example of such a study is the work of Rind et al. (1988a, b), in which the initial height and the intensity of GW depend on convection and large-scale wind shear.

The zonal mean wind tendencies induced by DSP GWD, OGWD and VD parameterizations are comparable with the results of other models that use these parameterizations (McFarlane et al., 1997; Norton and Thuburn, 1997; Manzini et al., 1997b). The structure of the tendencies induced by DSP GWD shows that it is not possible to parameterize adequately zonal wind DSP GWD tendencies in terms of simple Rayleigh friction with the coefficient dependent on the height only. For example, we can see quite different absolute values of the DSP GWD tendency in January at 0.1 hPa around 40°N and 40°S, whereas the absolute values of zonal wind are similar for both locations.

The inclusion of a Rayleigh friction sponge layer instead of DSP GWD may be the reason why models cannot reproduce the equatorward shift of the westerly wind maximum with height in the winter hemisphere.

The consideration of model stationary waves and low-frequency internal variability in the stratosphere and mesosphere shows that OGWD leads to smaller amplitudes of the stationary waves

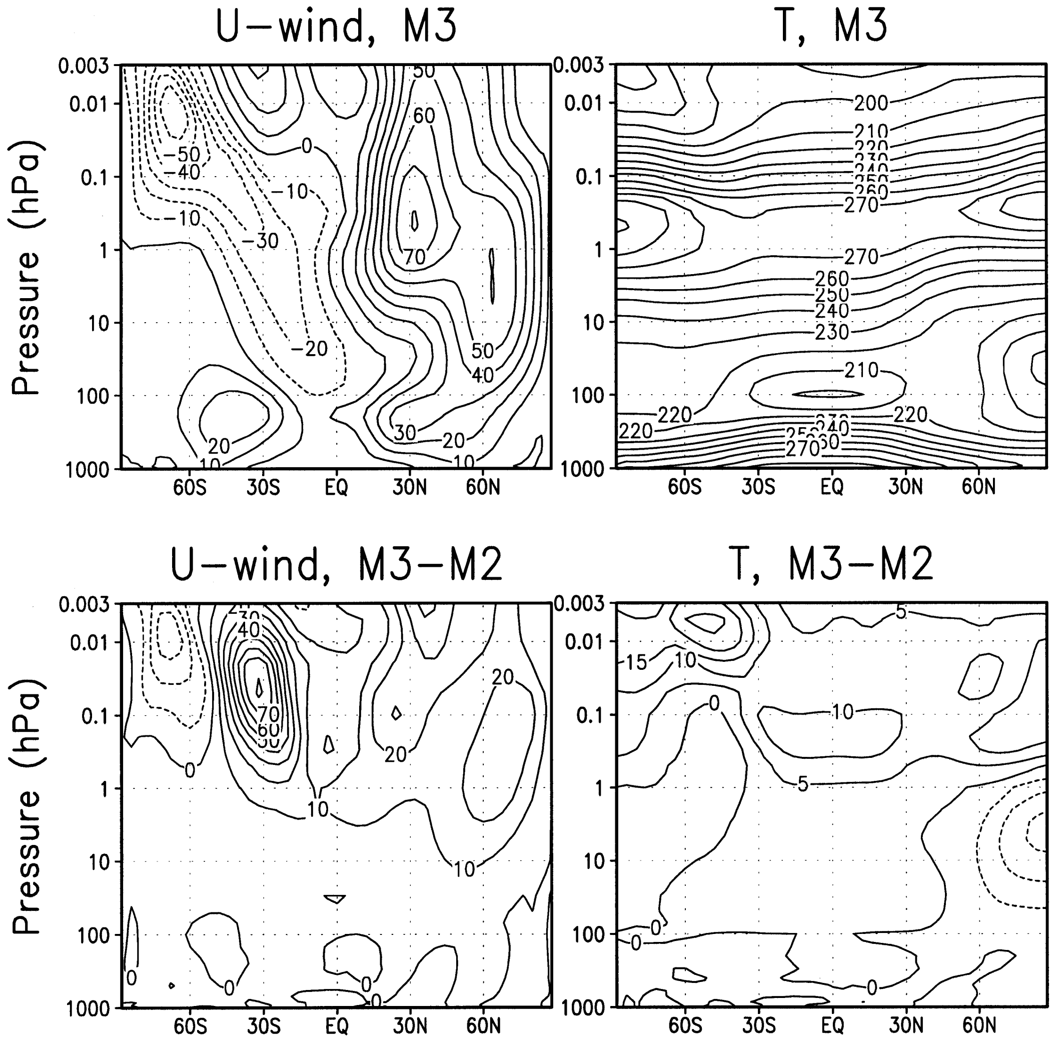

Fig. 10. Zonal mean zonal wind (top left) and temperature (top right) for M3; the difference of zonal wind (bottom left) and temperature (bottom right) between M3 and M2. Contour interval is 10 ms^{-1} for the wind, 10 K for mean temperature and 5 K for the difference of temperature.

and meridional fluxes. Assuming that main mechanism of low-frequency variability in winter stratosphere is the interaction between zonal mean flow and waves, smaller low-frequency variability in M2 than that in M1 is not surprising. Possible explanation of this behavior is a direct damping of stationary waves by OGWD. The model month-to-month variability in the stratosphere is weaker than that of Boville and Randel (1986), Pawson et al. (1995) and Butchart and Austin (1998). Such shortcomings can be induced by the underestimation of the amplitude of wave number 1 and the resulting stationary-wave heat flux. Another reason is an underestimation of variability in the troposphere. Kinetic energy of non-stationary eddies in the upper troposphere (at the level of 200 mb) is 2× weaker in the model than that in the observations. The main reason for such shortcomings is coarse horizontal resolution. In the troposphere, the low stratosphere model with 2× increased horizontal resolution (2.5° in longitude and 2° in latitude) kinetic energy of transient

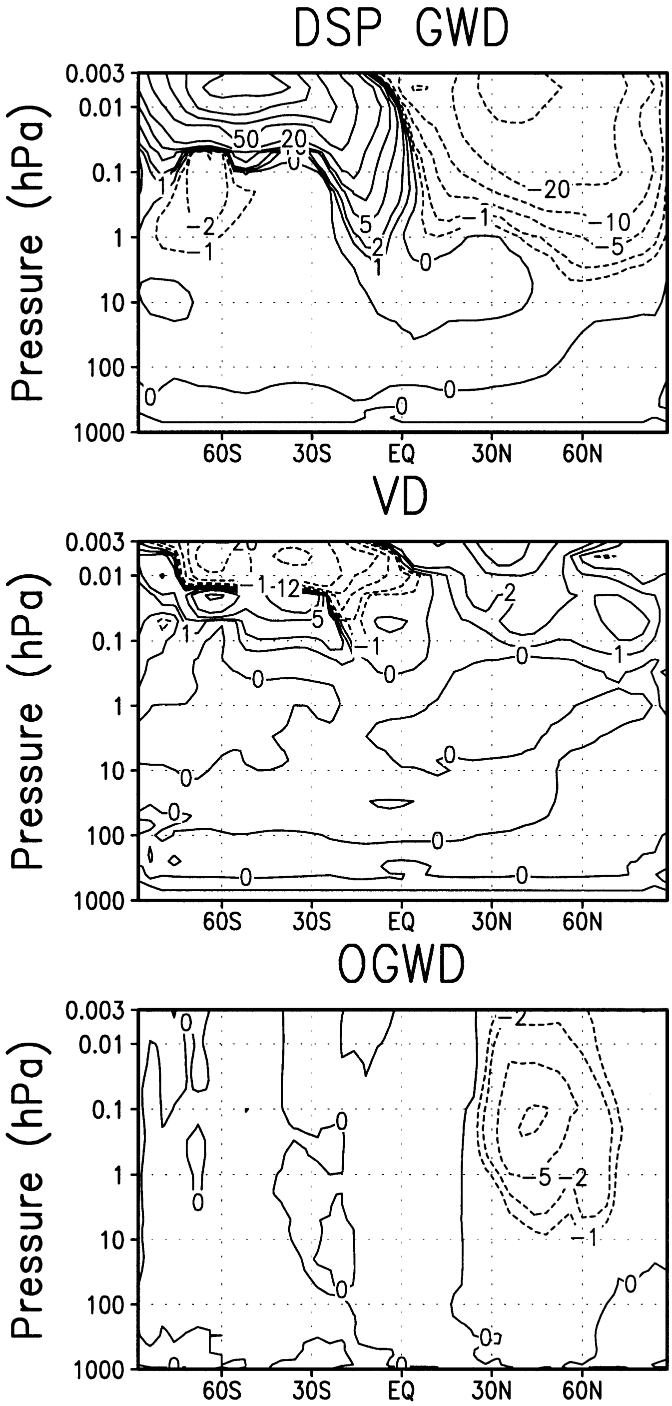

Fig. 11. Zonal mean tendencies for the zonal wind for M2 in January induced by: DSP GWD (top), VD (middle), OGWD (bottom). Contours are 0, ±1, ±2, ±5, ±10, ±20, ±50, ±100, ±150, ±200, ±250 $\mathrm{m\,s^{-1}\,day^{-1}}$. Negative contours are dashed.

eddies in the upper troposphere is almost the same as in the observations. The underestimation of wave number 1 in the troposphere is also the sequence of coarse resolution and insufficient eddy forcing. In the model with increased horizontal resolution, the amplitude of wave number 1 is almost the same as in the observations. Thus, extension of this model to the upper stratosphere and mesosphere can give a more realistic stratosphere climate than that in the model with coarse resolution. An additional reason for underestimation of low-frequency variability may be the absence of low-frequency variability resulting from external forcing, such as variability of sea-surface temperature, concentration of ozone and aerosols, variability of incoming ultra-violet radiation. Weak low-frequency variability also leads to underestimation of the development of stratospheric warmings. Only one major stratospheric warming is found in the 30-month run of M1.

The consideration of the first EOF of the zonal wind shows that in the northern hemispheric troposphere and stratosphere, it represents the wind anomalies with opposite sign in subtropics and high latitudes. The upper limit of this structure is at 1 hPa, and at higher levels, the structure is quite different. Probably, this restriction of the troposphere–stratosphere structure is imposed by DSP GWD tendency, which vanishes below 1 hPa. Inclusion the OGWD leads to restriction of this EOF structure above 10 hPa (not shown). In TSM AGCMs without any GWD, the meridional structure of the first EOF of the zonal wind remains nearly the same from the troposphere up to the upper model levels (Pawson et al., 1995; Koernich, 1998).

The structure of the first EOF of the temperature shows that in the stratosphere, the temperature anomalies at high latitudes are accompanied by anomalies of the other sign in low latitudes. This is in agreement with the results of Yulaeva et al. (1994).

7. Acknowledgement

E. M. Volodin carried out this work during the stay at the Institute for Atmospheric Physics. His participation in this study is supported by Russian Fund of Basic Research, grants 99-05-65533, 99-05-65442. The authors would like to thank E. Becker and A. Gabriel for valuable discussions and for carefully reading an earlier version of this manuscript. Our thanks are due to W. Randel for allowing us to use the data of stratospheric analysis, and to two anonymous referees for useful suggestions.

REFERENCES

Alekseev, V. A., Volodin, E. M., Galin, V. Ya., Dymnikov, V. P. and Lykossov, V. N. 1998. Modeling of the present-day climate by the atmospheric model of INM RAS "DNM GCM". *Description of the model version A5421 and results of AMIP II simulations. INM report N2086-B98*. Available by request from the address: Volodin, E. M., Institute of Numerical Mathematics, Gubkina 8, Moscow 117951 GSP-1, Russia.

Arakawa, A. and Lamb, V. R. 1981. A potential enstrophy and energy conserving scheme for shallow water equations. *Mon. Wea. Rev.* **109**, 18–36.

Betts, A. K. 1986. A new convective adjustment scheme. Part I. Observational and theoretical basis. *Quart. J. Roy. Met. Soc.* **112**, 677–691.

Boville, B. A. 1995. Middle atmosphere version of CCM2 (MACCM2): Annual cycle and interannual variability. *J. Geophys. Res.* **100**, 9017–9039.

Boville, B. A. and Randel, W. J. 1986. Observations and simulations of the variability of the stratosphere and troposphere in January. *J. Atmos. Sci.* **43**, 3015–3034.

Briegleb, B. P. 1992. Delta-Eddington approximation for solar radiation in the NCAR community climate model. *J. Geophys. Res.* **97**, 7603–7612.

Butchart, N. and Austin, J. 1998. Middle atmosphere climatologies from troposphere–stratosphere–mesosphere configuration of the UKMO's unified model. *J. Atmos. Sci.* **55**, 2782–2809.

Chou, M. D. and Kouvaris, L. 1991. Calculation of transmission functions in the infrared CO_2 and O_3 bands. *J. Geophys. Res.* **96**, 9003–9012.

Christiansen, B., Guldberg, A., Hansen, A. W. and Riishojgaard, L. P. 1997. On the response of a three-dimensional general circulation model to imposed changes in the ozone distribution. *J. Geophys. Res.* **102**, 13,051–13,077.

Galin, V. Ya. 1998. Parameterization of radiative processes in the DNM atmospheric model. *Izvestia AN. Fizika Atmosfery i Oceana* **34**, 380–389.

Fleming, E. L., Chandra, S., Barnett, J. J. and Corney, M. 1990. Zonal mean temperature, pressure, zonal wind and geopotential height as functions of latitude. *Adv. Space Res.* **10**, 1211–1259.

Hamilton, K. 1995. Interannual variability in the Northern Hemisphere winter middle atmosphere in control and perturbed experiments with the GFDL SKYHI general circulation model. *J. Atmos. Sci.* **52**, 44–66.

Hamilton, K. 1996. Comprehensive meteorological modeling of the middle atmosphere: a tutorial review. *J. Atm. Terr. Phys.* **58**, 1591–1627.

Hamilton, K. 1997. Gravity wave processes. Their parameterization in global climate models. NATO ASI Series. Series I. *Global Environmental Change* **50**, 480 pp.

Hamilton, K., Wilson, R. J., Mahlman, J. D. and Umscheid, L. J. 1995. Climatology of the SKYHI troposphere–stratosphere–mesosphere general circulation model. *J. Atmos. Sci.* **52**, 5–43.

Hines, C. O. 1997a. Doppler spread parameterization of gravity wave momentum deposition in the middle atmosphere. Part 1. Basic formulation. *J. Atm. Sol. Terr. Phys.* **59**, 371–386.

Hines, C. O. 1997b. Doppler spread parameterization of gravity wave momentum deposition in the middle atmosphere. Part 1. Broad and quasimonochromatic spectra, and implementation. *J. Atm. Sol. Terr. Phys.* **59**, 387–400.

Kalnay, E. et al. 1996. The NCEP/NCAR 40-year reanalysis project. *Bulletin of the American Meteorological Society* **77**, 437–471.

Koernich, H. 1998. *Die Klimaveraenderlichkeit in einem einfachen globalen Zirkulationmodell unter Beruecksichtigung der Orographie*. Diplomarbeit. University of Rostock, Germany.

Langematz, U. and Pawson, S. 1997. The Berlin troposphere–stratosphere–mesosphere GCM. Climatology and forcing mechanisms. *Quart. J. Royal Met. Soc.* **123**, 1075–1096.

Lindzen, R. S. 1981. Turbulence and stress owing to gravity wave and tidal breakdown. *J. Geophys. Res.* **86**, 9707–9714.

Manzini, E. and Bengtsson L. 1996. Stratospheric climate and variability from a general circulation model and observations. *Climate Dyn.* **12**, 615–639.

Manzini, E., McFarlane, N. A. and McLandress, C. 1997a. Impact of the Doppler-spread parameterization on the simulation of the middle atmosphere circulation using the MAECHAM4 general circulation model. *J. Geophys. Res.* **102**, 751–762.

Manzini, E., McFarlane, N. A. and McLandress, C. 1997b. Middle atmosphere simulations with the ECHAM4 model: Sensitivity to the Doppler spread gravity wave parameterization. In: *Gravity wave processes. Their parameterization in global climate models.* Edited by Hamilton, K. NATO ASI Series. Series I. *Global Environmental Change* **50**, 367–381.

Manzini, E. and McFarlane, N. A. 1998. The effect of varying the source spectrum of a gravity wave parameterization in a middle atmosphere circulation model. *J. Geophys. Res.* **103**, 31,523–31,539.

McFarlane, N., McLandress, C. and Beagley, S. 1997. Seasonal simulation with the Canadian Middle Atmosphere Model: Sensitivity to a combination of orographic and Doppler spread parameterizations of gravity wave drag. In: *Gravity wave processes. Their parameterization in global climate models.* Edited by Hamilton, K. NATO ASI Series. Series I. *Global Environmental Change* **50**, 351–366.

Norton, W. A. and Thuburn, J. 1997. The mesosphere in the extended UGAMP GCM. In: *Gravity wave processes. Their parameterization in global climate models.* Edited by Hamilton, K. NATO ASI Series. Series I. *Global Environmental Change* **50**, 383–401.

Palmer, T. N., Shutts, G. J. and Swinbank, R. 1986. Alleviation of a systematic westerly bias in general circulation and numerical weather prediction models through an orographic gravity wave drag parameterization. *Quart. J. Roy. Met. Soc.* **112**, 1001–1031.

Pawson, S. and Fiorino, M. 1998. A comparison of reanalyses in the tropical stratosphere. Part 1: thermal structure and the annual cycle. *Climate Dyn.* **14**, 631–644.

Pawson, S., Meyer, A. and Leder, S. 1995. Internal variability in a perpetual January integration of a troposphere–stratosphere–mesosphere GCM. *Quart. J. Roy. Met. Soc.* **121**, 369–397.

Pawson, S., Langematz, U., Radek, G, Schlese, U. and Strauch, P. 1998. The Berlin troposphere–stratosphere–mesosphere GCM. Sensitivity to physical parameterizations. *Quart. J. Roy. Met. Soc.* **124**, 1343–1371.

Randel, W. J. 1992. *Global atmospheric circulation statistics 1000-1 mb.* NCAR Technical Note, NCAR/TN-295+STR. National Center for Atmospheric Research, Boulder, Colorado.

Rind, D., Suozzo, R., Balachandran, N. K., Lacis, A. and Russel, G. 1988a. The GISS Global Climate Middle Atmosphere model. Part 1. Model structure and climatology. *J. Atmos. Sci.* **45**, 329–370.

Rind, D., Suozzo, R. and Balachandran, N. K. 1988b. The GISS Global Climate Middle Atmosphere model. Part 2. Model variability due to interactions between planetary waves, the mean circulation and gravity wave drag. *J. Atmos. Sci.* **45**, 371–386.

Swinbank, R., Lahoz, W. A., O'Neill, A., Douglas, C. S., Heaps, A. and Podd, D. 1998. Middle atmosphere variability in the UK Meteorological Office Unified Model. *Quart. J. Roy. Met. Soc.* **124**, 1485–1527.

Volodin, E. M. and Lykossov, V. N. 1998. Parameterization of heat and moisture transfer in the soil-vegetation system for use in atmospheric general circulation models: 1. Formulation and simulations based on local observational data. *Izvestia Akademii Nauk. Fizika Atmosfery i Okeana* **34**, 453–465.

Wang, W. C., Liang, X. Z., Dudek, M. P., Pollard, D. and Thompson, S. L. 1995. Atmospheric ozone as a climate gaz. *Atmos. Res.* **37**, 247–256.

Yulaeva, E., Holton, J. R. and Wallace, J. M. 1994. On the cause of the annual cycle in tropical lower-stratospheric temperatures. *J. Atmos. Sci.* **51**, 169–174.